

Effects of topological defects and local curvature on the electronic properties of planar graphene

Alberto Cortijo¹ and María A. H. Vozmediano²

¹*Unidad Asociada CSIC-UC3M, Instituto de Ciencia de Materiales de Madrid, CSIC, Cantoblanco, E-28049 Madrid, Spain.*

²*Unidad Asociada CSIC-UC3M, Universidad Carlos III de Madrid, E-28911 Leganés, Madrid, Spain.*

(Dated: March 23, 2022)

A formalism is proposed to study the electronic and transport properties of graphene sheets with corrugations as the one recently synthesized. The formalism is based on coupling the Dirac equation that models the low energy electronic excitations of clean flat graphene samples to a curved space. A cosmic string analogy allows to treat an arbitrary number of topological defects located at arbitrary positions on the graphene plane. The usual defects that will always be present in any graphene sample as pentagon-heptagon pairs and Stone-Wales defects are studied as an example. The local density of states around the defects acquires characteristic modulations that could be observed in scanning tunnel and transmission electron microscopy.

PACS numbers: 75.10.Jm, 75.10.Lp, 75.30.Ds

I. INTRODUCTION.

The recent synthesis of single layers of graphite and the experimental confirmation of the properties predicted by continuous models based on the Dirac equation[1, 2] have renewed the interest in this type of materials. Under a theoretical point of view, graphene has received a lot of attention in the past because it constitutes a beautiful and simple model of correlated electrons in two dimensions with unexpected physical properties[3]. A tight-binding method applied to the honeycomb lattice allows to describe the low energy electronic excitations of the system around the Fermi points by the massless Dirac equation in two dimensions. The density of states turns out to be zero at the Fermi points making useless most of the phenomenological expressions for transport properties in Fermi liquids. Among the unexpected properties are the anomalous behavior of the quasiparticles decaying linearly with frequency[4], and the so-called axial anomaly [5, 6] that has acquired special relevance in relation with the recently measured anomalous Hall effect in graphene[1, 2, 7].

Disorder plays a very important role in the electronic properties of low dimensional materials. In graphene and fullerenes the effect is even more drastic due to the vanishing of the density of states at the Fermi level. It is also an essential ingredient to search for the elusive magnetic behavior [8]. The influence of disorder on the electronic properties of graphene has been intensely studied recently. The classical works of disordered systems described by two dimensional Dirac fermions[9, 10, 11, 12] has been supplemented with an analysis of vacancies, edges and cracks[13].

Substitution of an hexagon by other type of polygon in the lattice without affecting the threefold coordination of the carbon atoms leads to the warping of the graphene sheet and is responsible for the formation of fullerenes. These defects can be seen as disclinations of the lattice which acquires locally a finite curvature. The accumulations of various defects may lead to closed shapes. Rings with $n < 6$ sides give rise to positively curved structures, the most popular being the C_{60} molecule that has twelve pentagons. Polygons with $n > 6$ sides lead to negative curvature as occur at the joining part of carbon nanotubes of different radius and in the Schwarzite[14], a structure appearing in many forms of carbon nanofoam[15]. This type of defects have been observed in experiments with carbon nanoparticles[16, 17, 18] and other layered materials[19]. Conical defects with an arbitrary opening angle can be produced by accumulation of pentagons in the cone tip and have been observed in [20, 21]. Inclusion of an equal number of pentagons and heptagonal rings in a graphene sheet would keep the flatness of the sheet at large scales and produce a flat structure with curved portions that would be structurally stable and have distinct electronic properties. This lattice distortions give rise to long range modifications in the electronic wave function. The change of the local electronic structure induced by a disclination is then very different from that produced by a vacancy or other impurities modelled by local potentials.

In this work we propose a model to study the electronic properties of a graphene sheet with an arbitrary number of topological defects that produce locally positive or negative curvature to the graphene sheet. We will first perform a complete description of the effect of disclinations on the low energy excitations of graphene, write down the most general model, and solve it to find the corrections to the density of states induced by heptagon-pentagon pairs and Stone-Wales defects.

Disclinations can be included in the continuous model as topological vortices coupled to electronic excitations. We will show that certain types of disclinations produce a non-vanishing local density of states at Fermi level. In the

average flat sheet of slightly curved graphene, heptagon-pentagon pairs can be described as bound in dislocations that change the electronic properties of the system. The electronic properties induced by single defects depend crucially on the nature of the substitutional polygon. Topological defects that involve the exchange of the Fermi points (substitution of an hexagon by an odd-membered ring) can break the electron-hole symmetry of the system and enhance the local density of states that remains zero at the Fermi level. The situation is similar to the effects found in the study of vacancies in the tight binding model when next to nearest neighbors (t') are included[13]. Defects involving even-membered rings induce a non zero density of states at the Fermi level preserving the electron-hole symmetry. An arbitrary number of heptagon-pentagon pairs produce characteristic patterns in the local density of states that can be observed in scanning tunnel (STM)[22] and electron transmission spectroscopy (ETS). The results obtained can help to interpret recent Electrostatic Force Microscopy (EFM) measurements that indicate large potential differences between micrometer large regions on the surface of highly oriented graphite[23].

The rest of the paper is organized as follows: in Sect. 2 we review briefly the main features of the continuous model of graphene based on the Dirac equation. We make special emphasis on the internal symmetries that will be affected by the inclusion of topological defects. In Sect. 3 single disclinations are introduced in the model by means of gauge fields as a warmup exercise and as a way to show the limitations of the model. Substitution of an hexagon by an even-membered ring is shown to induce a finite density of states at the Fermi level. Section 4 contains the main results of the paper. A formalism is presented that permits to study an arbitrary number of defects located at given positions in the graphene lattice. The model is based on the observation that the effect of a cosmic string on the space-time is the same as the one produced by a pentagon in the two-dimensional graphene plane. We generalize the cosmic string formalism to include the effects of defects with an "excess angle" such as heptagons and propose a metric to describe an arbitrary number of disclinations in the graphene plane. The electronic properties of the model are obtained from the Greens function of the system in the given metric. We then apply the method to study the type of defects that are most probably present in graphene samples: heptagon-pentagon pairs and Stone-Wales defects. The main results are shown in section 5. We show the inhomogeneous structures produced in the density of states by these defects and argue that they can be observed in STM experiments. The last section contains the conclusions and open problems. Appendices A and B contain the technical details of the calculations of sections 3 and 4 respectively.

II. LOW ENERGY DESCRIPTION OF GRAPHENE.

The conduction band of graphene is well described by a tight binding model which includes the π orbitals which are perpendicular to the plane at each C atom[24, 25]. This model describes a semimetal, with zero density of states at the Fermi energy, and where the Fermi surface is reduced to two inequivalent K-points located at the corner of the hexagonal Brillouin Zone.

The low-energy excitations with momenta in the vicinity of any of the Fermi points K_+ and K_- have a linear dispersion and can be described by a continuous model which reduces to the Dirac equation in two dimensions[26, 27, 28]. In the absence of interactions or disorder mixing the two Fermi points, the electronic properties of the system are well described by the effective low-energy Hamiltonian density:

$$\mathcal{H}_{0i} = \hbar v_F \int d^2\mathbf{r} \bar{\Psi}_i(\mathbf{r}) (i\sigma_x \partial_x + i\sigma_y \partial_y) \Psi_i(\mathbf{r}) , \quad (1)$$

where $\sigma_{x,y}$ are the Pauli matrices, $v_F = (3ta)/2$, and $a = 1.4\text{\AA}$ is the distance between nearest carbon atoms. The components of the two-dimensional wavefunction:

$$\Psi_i(\mathbf{r}) = \begin{pmatrix} \varphi_A(\mathbf{r}) \\ \varphi_B(\mathbf{r}) \end{pmatrix} \quad (2)$$

correspond to the amplitude of the wave function in each of the two sublattices (A and B) which build up the honeycomb structure. We will later show that the parameter space where this spinorial degree of freedom acts is the polar angle of the real space of the graphene plane. The dispersion relation $\epsilon(\mathbf{k}) = v_F |\mathbf{k}|$ gives rise to the density of states

$$\rho(\omega) = \frac{8}{v_F^2} |\omega|$$

which vanishes at the Fermi level $\omega = 0$. The electronic states attached to the two inequivalent Fermi points will be independent in the absence of interactions that mix the two points.

The type of defects that we will study affect the microscopic description of graphene in all possible ways: induce local curvature to the sheet, can mix the two triangular sublattices, and can exchange the two Fermi points. It

is then convenient to set a unified description and combine the bispinor attached to each Fermi point (what is called in semiconductors language the valley degeneracy) into a four component Dirac spinor. We will do that and then analyze the behavior of these pseudospinors under rotations what will be crucial in the study of the boundary conditions imposed by the defects.

The four dimensional Hamiltonian is

$$H_D = -iv_F\hbar(1 \otimes \sigma_1 \partial_x + \tau^3 \otimes \sigma_2 \partial_y), \quad (3)$$

where σ and τ matrices are Pauli matrices acting on the sublattice and valley degree of freedom respectively. The dispersion relation associated to (3) is

$$E(\mathbf{p}) = \pm \hbar v_F |\mathbf{p}| \equiv \pm \hbar v_F p. \quad (4)$$

The solutions of the Dirac equation - with positive energy - are of the form

$$\Psi_{E>0} = \exp(i\mathbf{p}\mathbf{r}) \begin{pmatrix} e^{-i\theta/2} \\ e^{i\theta/2} \\ e^{i\theta/2} \\ e^{-i\theta/2} \end{pmatrix}, \quad (5)$$

where θ is the polar angle of the vector \mathbf{p} in real space. The first (second) two components of (5) refer to the bispinor around K_+ (K_-).

The behavior of (5) under a real space rotation of angle α around the oz axis is

$$\Psi'(\mathbf{r}') = \Psi'(R^{-1}\mathbf{r}) \equiv T_R \Psi(R^{-1}\mathbf{r}). \quad (6)$$

the transformation $\mathbf{p}' = \mathbf{p}R = p(\cos(\alpha + \theta), \sin(\alpha + \theta))$, determines the T_R matrix to be

$$T_R = \begin{pmatrix} \exp(i\frac{\alpha}{2}\sigma_3) & 0 \\ 0 & \exp(-i\frac{\alpha}{2}\sigma_3) \end{pmatrix}, \quad (7)$$

what shows that (5) transforms as a real spinor under spacial rotations of the graphene plane. Each of the two-dimensional K-spinor transform under the given rotation with the matrix $\pm\sigma_3/2$. This opposite sign is often referred to as the K-spinors having opposite chirality or helicity.

III. EFFECT OF A SINGLE DISCLINATION

Substitution of an hexagon by an n-sided polygon in the graphene lattice can be described by a cut-and-paste procedure as the one shown in fig. 1 for the particular case of a pentagon. A $\pi/3$ sector of the lattice is removed and the edges are glued. In this case the planar lattice acquires the form of a cone with the pentagon in its apex. Such a disclination has two distinct effects on the graphene sheet. It induces locally positive (negative) curvature for $n < 6$ ($n > 6$) and, in the paste procedure, it can break the bipartite nature of the lattice if n is odd while preserving the symmetry if n is even. This makes a difference with the case of the formation of nanotubes where the bipartite nature of the lattice always remains intact. The presence of an odd-membered ring means that the two fermion flavors defined in eq. (2) are also exchanged when moving around such a defect[26]. The scheme to incorporate this change in a continuous description was discussed in refs. [27] and [29]. The process can be described by means of a non Abelian gauge field, which rotates the spinors in flavor space. As will be shown the two cases have very different effect on the density of states of the system. Conical defects with an arbitrary opening angle made by accumulation of pentagons at the tip have been observed experimentally in[20].

We shall begin describing the effect on the density of states produced by conical defects that do not alter the bipartite character of the hexagonal lattice.

A spinor defined in a plane without topological defects acquires a phase of π (changes sign) when going around a closed path[30]. In the two-dimensional description this can be written as

$$\psi_0(\mathbf{r}, \varphi = 2\pi) = e^{i\pi\sigma_3} \psi_0(\mathbf{r}, \varphi = 0).$$

When the spinor rotates around a defect with a deficit angle $b = 2\pi b$ it obeys the boundary condition

$$\psi(\mathbf{r}, \varphi = 2\pi) = e^{i2\pi(1-b)\frac{\sigma_3}{2}} \psi(\mathbf{r}, \varphi = 0).$$

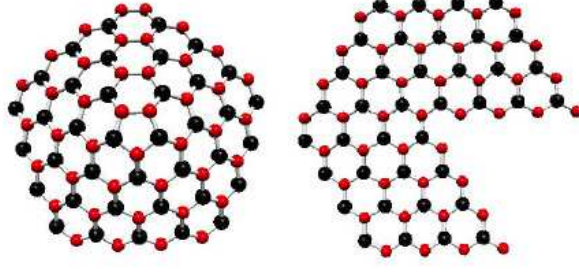


FIG. 1: Left: Effect of a pentagonal defect in a graphene layer. Right: Cut-and-paste procedure to form the pentagonal defect. The points at the edges are connected by a link what induces a frustration of the bipartite character of the lattice at the seam.

We can convert the phase b in a continuous variable and assume that a lattice distortion which rotates the lattice axis can be parametrized by the angle of rotation, $\theta(\mathbf{r})$, of the local axes with respect to a fixed reference frame. The spinor can be written as

$$\psi(\mathbf{r}, \varphi) = e^{i(\int_x \mathbf{A}(\mathbf{y}) d\mathbf{y}) \frac{\sigma_3}{2}} \psi_0(\mathbf{r}, \varphi), \quad (8)$$

with

$$\mathbf{A}(\mathbf{r}) \sim \nabla \theta(\mathbf{r}).$$

In the four-dimensional representation, applying the Dirac operator $i\gamma \cdot \nabla$ to eq. (8) we get the following hamiltonian:

$$H = -i\hbar v_F \vec{\gamma} \cdot \vec{\partial} + g \gamma^q \vec{\gamma} \cdot \vec{A}(\mathbf{r}), \quad (9)$$

where v_F is the Fermi velocity, γ^i are 4×4 matrices constructed from the Pauli matrices, $\gamma^q = \frac{\sigma_3}{2} \otimes I$, the latin indices run over the two spatial dimensions and g is a coupling parameter. The external field $A_i(\vec{r})$ takes the form of a vortex

$$A^j(\vec{r}) = \frac{\Phi}{2\pi} \epsilon^{3ji} \frac{x_i}{r^2} \quad (10)$$

The constant Φ is a parameter that represents the strength of the vortex: $\Phi = \oint \vec{A} d\vec{r}$ and is related to the opening angle of the defect. A geometric formulation of the same problem has been given recently in [31] in terms of holonomy. In the case of an odd-membered ring, the two Fermi points are also exchanged[27] what can be modelled by using a non-abelian gauge potential that rotates the spinors in the $SU(2)$ space of the Fermi points. In this case an extra matrix appears in the coupling of the gauge field in (9). In what follows we will consider the static vortex as an external gauge potential. This approximation is justified by the fact that the dynamics of the defects in the lattice is related to the σ bonds with energy of about 4 eV whereas the electronic excitations described by the spinors involve energies of the order of 20 meV. We will then use time-independent perturbation theory to calculate corrections to the self-energy $\Sigma(\mathbf{k}, \omega)$ in the weak coupling regime of the parameter

$$\hat{g} \equiv \frac{\Phi}{2\pi L^2},$$

where L is the dimension of the sample. The correction to the density of states induced by the defect is obtained from the self-energy by

$$\rho(\omega) = \frac{1}{\pi} \text{Im} \int \text{Tr} G(\omega, \mathbf{k})$$

The presence of the defect breaks the translational invariance and the computation of the density of states deviates slightly from the standard path. The details of the calculation are given in appendix A.

The correction to the density of states given in (A4) is shown in Fig. 2 for several values of the coupling parameter \hat{g} . We see that the defect induces a non-zero density of states at the Fermi energy given by

$$\rho(\omega = \varepsilon_F, |\hat{g}|) = \frac{2\sqrt{|\hat{g}|}}{v_F}. \quad (11)$$

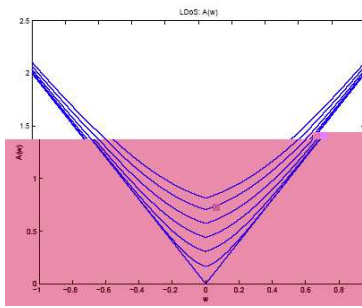


FIG. 2: Total density of states for an even-membered ring for several increasing values of \hat{g} (see text) in arbitrary units starting with $\hat{g}=0$.

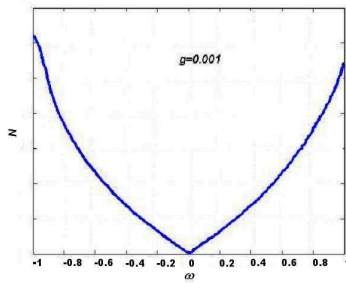


FIG. 3: Total density of states for an odd-membered ring.

The value of the DOS increases with the curvature (encoded in the parameter \hat{g}). It depends on the size of the sample and will go to zero as $(1/L)$ in the thermodynamic limit. Similar results were obtained in [32] and [33] where the same problem is addressed but there they compute the local DOS around a defect truncating the singularity at the apex of the cone. Numerical ab initio calculations show sharp resonant peaks in the LDOS at the tip apex of nanocones [34, 35] that have been proposed for electronic applications in field emission devices. In both cases the computations refer to the local density of states.

The case of an odd membered ring is technically more involved in our formalism and we have not obtained an analytical result. The complication is produced by the extra matrix needed to exchange the two fermion flavors. A numerical integration of the DOS for this case is shown in fig. 3 for the case of a single pentagonal defect. We can see that the DOS at the Fermi level is zero in this case also in agreement with [32] and [33]. We can also appreciate a small deviation from the perfect electron-hole symmetry of $\rho(\omega)$. The slope of the curve at the origin suggests an enhancement of the DOS around the zero energy what would agree with the STM observations described in [21]. We will come back to the single defect in the next section.

IV. AN ARBITRARY NUMBER OF DEFECTS AT GIVEN POSITIONS IN THE LATTICE.

An alternative approach to the gauge theory of defects discussed in the previous section is to include the local curvature induced by an n -membered ring by coupling the Dirac equation to a curved space. In this context one can see that the substitution of a hexagon by a polygon of $n < 6$ sides gives rise to a conical singularity with deficit angle $(2\pi/6)(6 - n)$. This kind of singularities have been studied in cosmology as they are produced by cosmic strings, a type of topological defect that arises when a $U(1)$ gauge symmetry is spontaneously broken[36]. We can obtain the correction to the density of states induced by a set of defects with arbitrary opening angle by coupling the Dirac equation to a curved space with an appropriate metric as described in ref. [37]. In this section we will closely follow the formalism set in these reference.

The metric of a two dimensional space in presence of a single cosmic string in polar coordinates is:

$$ds^2 = -dt^2 + dr^2 + c^2 r^2 d\theta^2, \quad (12)$$

where the parameter c is a constant related to the deficit angle by $c = 1 - b$.

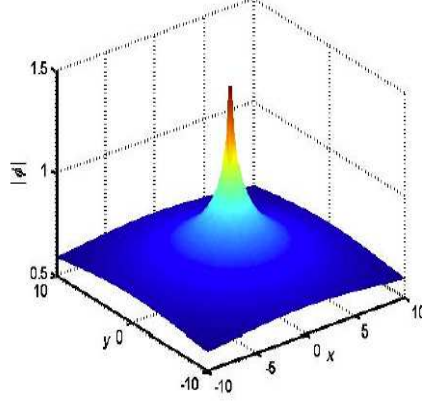


FIG. 4: Electronic density around a conical defect.

The dynamics of a massless Dirac spinor in a curved spacetime is governed by the Dirac equation:

$$i\gamma^\mu \nabla_\mu \psi = 0 \quad (13)$$

The difference with the flat space lies in the definition of the γ matrices that satisfy generalized anticommutation relations

$$\{\gamma^\mu, \gamma^\nu\} = 2g^{\mu\nu},$$

and in the covariant derivative operator, defined as

$$\nabla_\mu = \partial_\mu - \Gamma_\mu$$

where Γ_μ is the spin connection of the spinor field that can be calculated using the tetrad formalism[38]. The present formalism can help to clarify the nature of the states appearing at the Fermi level in fig. 2. Fig. 4 shows the solution of the Dirac equation (13) in the presence of a single defect with a positive deficit angle (positive curvature). The electronic density is strongly peaked at the position of the defect suggesting a bound state but the behavior at large distances is a power law with an angle-dependent exponent less than two which corresponds to a non normalizable wave function. This behavior is similar to the one found in the case of a single vacancy[39] and suggests that a system with a number of this defects with overlapping wave functions will be metallic.

The case of a single cosmic string which represents a deficit angle in the space can be generalized to describe seven membered rings representing an angle surplus by considering a value for c larger than 1. This situation is non-physical from a general relativity viewpoint as it would correspond to a string with negative mass density but it makes perfect sense in our case. The scenario can also be generalized to describe an arbitrary number of pentagons and heptagons by using the following metric:

$$ds^2 = -dt^2 + e^{-2\Lambda(x,y)}(dx^2 + dy^2), \quad (14)$$

where

$$\Lambda(\mathbf{r}) = \sum_{i=1}^N 4\mu_i \log(r_i)$$

and

$$r_i = [(x - a_i)^2 + (y - b_i)^2]^{1/2}.$$

This metric describes the space-time around N parallel cosmic strings, located at the points (a_i, b_i) . The parameters μ_i are related to the angle defect or surplus by the relationship $c_i = 1 - 4\mu_i$ in such manner that if $c_i < 1 (> 1)$ then $\mu_i > 0 (< 0)$.

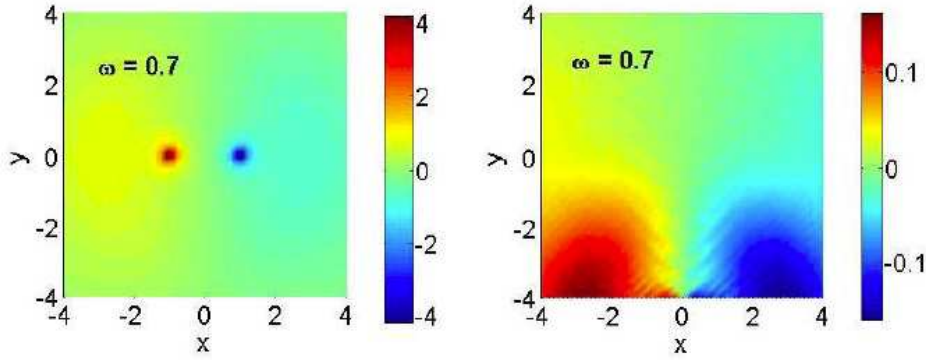


FIG. 5: Left: Image of the local density of states in a large portion of the plane with a heptagon-pentagon pair located at the center. Green color represents the DOS of the flat graphene sheet. Right: Same with the defect located out of plane.

From equation (13) we can write down the Dirac equation for the electron propagator, $S_F(x, x')$:

$$i\gamma^\mu(\mathbf{r})(\partial_\mu - \Gamma_\mu)S_F(x, x') = \frac{1}{\sqrt{-g}}\delta^3(x - x'), \quad (15)$$

where $x = (t, \mathbf{r})$. The local density of states $N(\omega, \mathbf{r})$ is obtained from (15) by Fourier transforming the time component and taking the limit $\mathbf{r} \rightarrow \mathbf{r}'$:

$$N(\omega, \mathbf{r}) = \text{ImTr}S_F(\omega, \mathbf{r}, \mathbf{r}). \quad (16)$$

We solve eq. (16) considering the curvature induced by the defects as a perturbation of the flat graphene layer. The details of the calculation are given in Appendix B. Here we will show the results obtained.

We must notice that the present formalism takes into account the effects produced by the local curvature of the lattice but does not include yet the effect of identifying points of different sublattices. It is then specially suitable to describe pentagon-heptagon pairs or Stone-Wales defects where the effect of the line of dislocation is minimized.

V. THE LOCAL DENSITY OF STATES.

In this section we will show the results obtained by applying the cosmic string formalism to various cases of physical interest. The left side of Fig. 5 shows the correction to the local density of states at fixed energy and for a large region of the graphene plane with a pentagon-heptagon pair in the middle. The color code is indicated in the figure: green stands for the DOS of perfect graphene at the given energy and red (blue) indicates an accumulation (depression) of the density in the area. We can see that pentagonal (heptagonal) rings enhance (depress) the electron density. A similar result has been obtained in [34] with numerical simulations. It is to note that a somehow contradictory result was obtained in [40] where they studied the electrostatics of a graphene plane with defects. They found that disclinations corresponding to rings with more (less) than six carbon atoms function as attractors (repellent) to point charges. In the latter approach they were concerned exclusively with the curvature effect not taking into account the connectivity of the lattice. It is obvious that this issue needs further investigation. The right hand side of Fig. 5 represents the structure of the density of states produced by the same defect located out of the plane in the lower part. Notice the different intensities in the two graphics. The dipolar character of the defect is clear. Fig. 6 illustrates the same phenomena in different coordinates. We show the contribution to the local density of states (LDOS) as a function of the energy coming from a pentagon-heptagon pair located at $(x = 0, y = \pm 1)$ computed at different points of the plane. We can see that the LDOS shows oscillations depending on the position of the point relative to the position of the defect. The correction is zero in the line perpendicular to the segment joining the two defects as can be seen in fig. ??.

The intensity of the oscillations grows with the energy. Fig. 7 shows the correction to the local density of states in a extended region of the lattice induced by two pairs of heptagon-pentagon defects located out of the region for increasing values of the energy. The first pair is located in the down-left diagonal direction approximately at coordinates $(-4.5, -4.5)$ of figure and the second pair is located approximately at $(4.5, 0)$. In fig. 7 a) in the space between the defects the LDOS is almost zero except at local zones where the correction is small (in the region in the

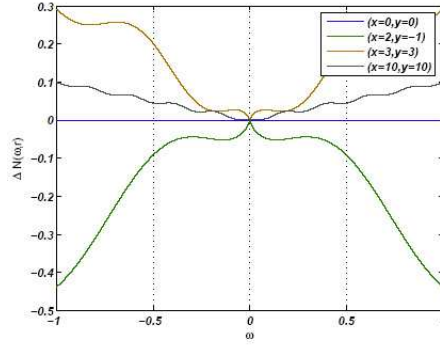


FIG. 6: Correction to the local density of states for different points of the lattice from a pentagon-heptagon pair located at $(x = 0, y = \pm 1)$.

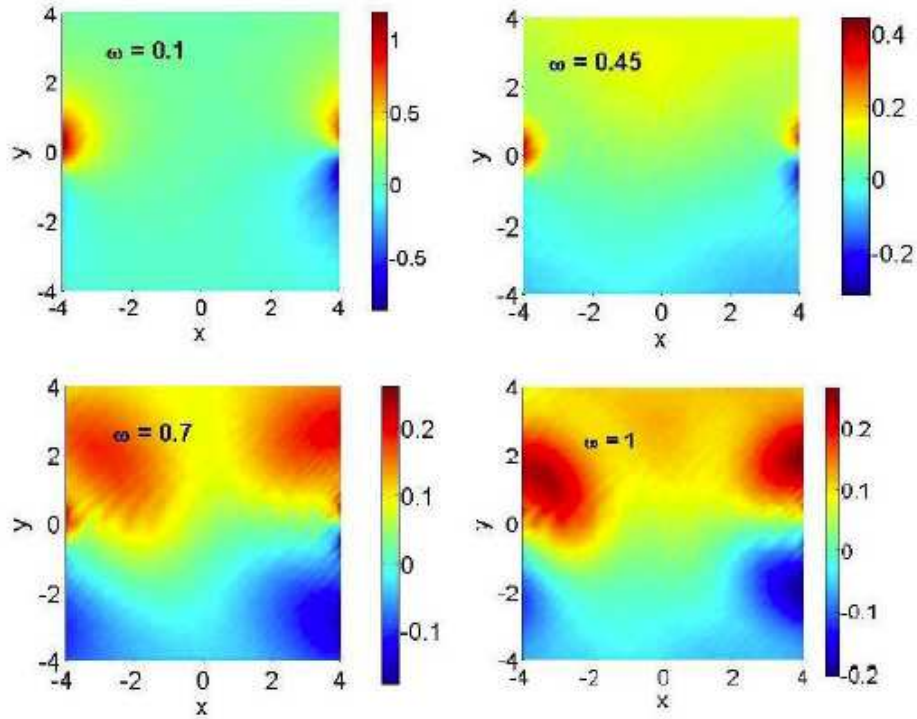


FIG. 7: Correction to the local density of states in a wide region around two pairs of heptagon-pentagon defects located out of the region (see text) for increasing values of the energy.

left down side the density is enhanced by the proximity of the defects). As the frequency increases up to $\omega = 1$ near to the energy cutoff (fig. 7c) the LDOS is enhanced and inhomogeneous oscillations can be observed in the region between the defects. The patterns depend also on the relative orientation of the dipoles. These type of structures can be observed in experiments of scanning tunnel spectroscopy. In general the intensity of the oscillations grows with the energy. Fig. 7 shows the relative correction (normalized to the free density of states) to the local density of states in a extended region of the lattice induced by two pairs of heptagon-pentagon defects located out of the region for increasing values of the energy. The first pair is located in the down-left diagonal direction approximately at coordinates $(-4.5, -4.5)$ of figure and the second pair is located approximately at $(4.5, 0)$. In fig. 7 a) in the space between the defects the LDOS is almost zero except at local zones where the correction is small (in the region in the left down side the density is enhanced by the proximity of the defects). As the frequency increases up to $\omega = 1$ near

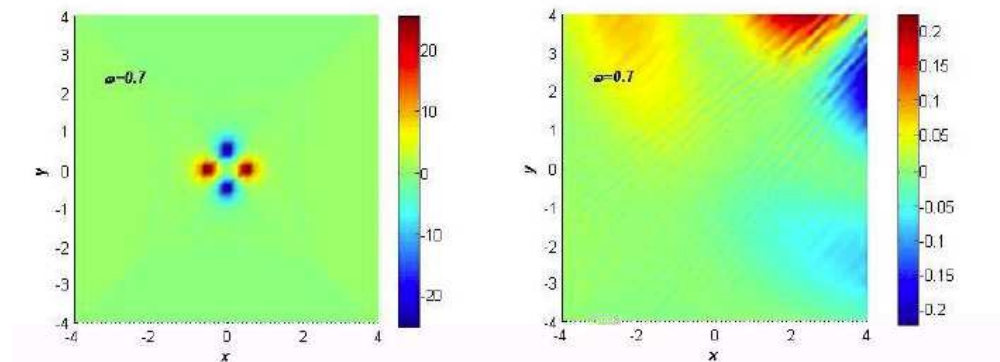


FIG. 8: Left: Local density of states around a Stone-Wales defect located at the center for a fixed value of the frequency. Right: same for a defect located out of plane (see text).

to the energy cutoff (fig. 7c) the LDOS is enhanced and inhomogeneous oscillations can be observed in a wide area around the defects. The patterns depend also on the relative orientation of the dipoles. The spacial extent of the correction is such that the intensity decays to ten percent in approximately 20 unit cells so they can be observed in scanning tunnel spectroscopy as inhomogeneous regions of a few nanometers.

Stone-Wales defects made of two adjacent heptagons and two pentagons are known to be energetically quasi-stable[41] and form naturally in experiments of ion bombarded nanotubes as a mechanism to reduce the dangling bonds in large vacancies[42]. They have received a lot of attention in carbon nanotubes where they strongly affect the electronic properties[43]. In graphene they have been shown to change the band structure causing a nondispersive spin-polarized band to form and a peak in the density of states close to the Fermi level[44]. They have also been shown recently to change substantially the electronic structure of hydrogen adsorbed in graphene[45]. In the left side of fig. 8 we show an image of an extended region of the graphene plane with a Stone-Wales defect located in the middle at a fixed intermediate frequency. The modulation of the local density of states around the defects is hardly noticeable due to the strong intensity localized at the defects. The same image is shown in the right hand side of fig. 8 with the Stone-Wales defect located out of plane in the upper right corner. The modulation of the LDOS is clearly visible.

VI. CONCLUSIONS AND OPEN PROBLEMS.

We have presented a formalism based on cosmic strings to study the electronic structure of a slightly warped graphene sheet where the local curvature is produced by substitution of an hexagon by an n -sided polygon with $n \neq 6$. This type of disorder induces long range forces in the graphene system and is very different from the most studied cases of vacancies, cracks, edges, etc. We have shown that the local density of states is enhanced around defects with $n < 6$ which induce positive curvature in the lattice while the charge is "repelled" from regions with negative curvature ($n > 6$). A single conical defect with an even number of hexagonal sides excised produces a finite DOS at the Fermi energy of a value that increases with the curvature of the defect in agreement with STM observations[21]. The zero energy electronic states are peaked at the defect but the wave function remains finite at large distances so they are extended states. Heptagon-pentagon pairs that keep the graphene sheet flat in the long range behave as dipoles and give rise to characteristic modulations of the DOS that can be observed by STM. The same behavior is induced by Stone-Wales defects which are expected to be produced by annealing of irradiated samples as observed in carbon nanotubes[42]. The magnitude of the oscillations increases with the frequency and the characteristic patterns could be used to characterize the graphene samples. The features predicted in this work should also be observable in other layered materials with similar structure as boron nitride[19]. The present analysis can help to clarify the issue of the analysis and interpretation of STM images.

VII. ACKNOWLEDGMENTS.

We thank B. Valenzuela, P. Guinea and P. Esquinazi for many illuminating discussions. A. C. thanks N. Ozdemir for kindly providing details of the calculations in ref. [37]. Funding from MCyT (Spain) through grant MAT2002-0495-C02-01 and from the European Union Contract No. 12881 (NEST) is acknowledged.

APPENDIX A: A SINGLE DEFECT

In a disordered system, in general, because of the presence of an external potential or impurities, the space is inhomogeneous. The Green's function doesn't depend on the difference $(\mathbf{r} - \mathbf{r}')$ and \mathbf{k} is no longer a good quantum number. If the external potential or the effect of the impurities are time-independent we have elastic scattering and the states \mathbf{k} and \mathbf{k}' have the same energy.

We want to calculate the total density of states $\rho(\omega)$ of the system perturbed by the defect via the vector potential given in eq. (10). This density is the imaginary part of the Green's function integrated over all positions, in the limit $\mathbf{r}' \rightarrow \mathbf{r}$:

$$\rho(\omega) = \int \text{Im} G(\omega, \mathbf{r}, \mathbf{r}) d\mathbf{r}.$$

In terms of the Green's function in momentum representation, $\rho(\omega)$ can be written as:

$$\rho(\omega) = \text{Im} \int \int \frac{d\mathbf{k}}{(2\pi)^2} \int \frac{d\mathbf{k}'}{(2\pi)^2} e^{i\mathbf{k}\mathbf{r}} e^{i\mathbf{k}'\mathbf{r}} G(\omega, \mathbf{k}, \mathbf{k}') d\mathbf{r}.$$

The integration over \mathbf{r} gives delta function $4\pi^2 \delta(\mathbf{k} + \mathbf{k}')$, and $\rho(\omega)$ then reads:

$$\rho(\omega) = \int \frac{d\mathbf{k}}{(2\pi)^2} \text{Im} G(\omega, \mathbf{k}, -\mathbf{k}).$$

With this expression we can compute ordinary Feynmann diagrams contributing to the self-energy $\Sigma(\omega, \mathbf{k}, \mathbf{k}')$, calculate the Green's function $G(\omega, \mathbf{k}, \mathbf{k}')$ and make the substitution $\mathbf{k}' = -\mathbf{k}$. The first order correction to the electron self-energy is

$$\Sigma(\mathbf{k}, \omega) = \Sigma_0(\mathbf{k}) + \hat{g} \gamma^i \gamma^i \langle \mathbf{k} | A_i(\vec{r}) | \mathbf{k} \rangle + O(g^2) \quad (\text{A1})$$

At this order the first contribution to the self-energy is simply the Fourier transform of the gauge potential eq. (10) and does not depend on ω . It turns out to be:

$$\Sigma(\mathbf{k}, \omega) \simeq v_F \gamma^i k_i + \hat{g} \gamma^i \frac{k_i}{k^2} \equiv v_F f(k^2) \gamma^i k_i, \quad (\text{A2})$$

where $f(k^2)$ is $f(k^2) = 1 + \frac{\hat{g}}{k^2}$. The two-point Green's function reads, at this level:

$$G(\omega, \mathbf{k}) = \frac{w + f \gamma^i k_i}{\omega^2 - f^2 k^2 + i\delta} \quad (\text{A3})$$

We compute the density of states of the system

$$\rho(\omega) = \text{Im} \int \text{Tr} G(\omega, \mathbf{k})$$

with the Green's function defined in eq. (A3). The result is

$$\rho(\omega) = \frac{4\omega v_F^4 (K^+(\omega))^4}{|v_F^4 (K^+(\omega))^4 - \hat{g}^2|}, \quad (\text{A4})$$

where $K^+(\omega) = \sqrt{\frac{1}{2}(2\hat{g} + v_F \omega^2 + \sqrt{\omega^4 + 2\omega^2 \hat{g} v_F})}$.

APPENDIX B: MULTIPLE DEFECTS

In the metric defined by (14):

$$g_{\mu\nu} = \begin{pmatrix} -1 & 0 & 0 \\ 0 & e^{-2\Lambda} & 0 \\ 0 & 0 & e^{-2\Lambda} \end{pmatrix}, \quad (\text{B1})$$

the gamma matrices and the spinor connection in the curved background are found to be

$$\gamma^0(\mathbf{r}) = \gamma^0, \quad \gamma^i(\mathbf{r}) = e^{\Lambda(\mathbf{r})} \gamma^i \quad (i = 1, 2)$$

$$\Gamma_1(\mathbf{r}) = -\frac{1}{2} \gamma^1 \gamma^2 \partial_y \Lambda, \quad \Gamma_2(\mathbf{r}) = -\frac{1}{2} \gamma^2 \gamma^1 \partial_x \Lambda,$$

and the determinant of the metric tensor is

$$\sqrt{-g} = e^{-2\Lambda}.$$

We solve eq. (15) by considering μ as a small parameter to perturb around the flat space. In the case that the defects are made of pentagon heptagon pairs the value of μ is $\mu_i \equiv \mu = 1/24$ ($b = 1/6$).

We expand the function $\Lambda(\mathbf{r})$ to first order in μ and get for the electron propagator the equation

$$i\gamma^0 \partial_0 S_F - i\gamma^j \partial_j S_F - V S_F = \delta^3(x - x'). \quad (\text{B2})$$

As before latin indices run over spatial dimensions. We can see that eq. (B2) is the equation for the Greens function of a spinor field in flat space but in an external potential V given by:

$$V(\omega, \mathbf{r}) = 2i\Lambda\gamma^0\partial_0 + i\Lambda\gamma^j\partial_j + \frac{i}{2}\gamma^j(\partial_j\Lambda). \quad (\text{B3})$$

As in the case of a single defect, the effect of the curvature has been traded to an external potential. In order to get the corrections to the density of states as a function of the frequency and position we perform a time fourier transform in (B2) and get an equation for the quantity $\hat{S}_F(\omega, \mathbf{r}, \mathbf{r}')$:

$$\gamma^0 \omega \hat{S}_F - i\gamma^j \partial_j \hat{S}_F - \hat{V} \hat{S}_F = \delta^2(\mathbf{r} - \mathbf{r}'), \quad (\text{B4})$$

where \hat{V} is the time fourier transform of the potential (B3). The first order correction to the propagator in real space is

$$\hat{S}_F^1(\omega, \mathbf{r}, \mathbf{r}') = \int d^2 r'' \hat{S}_F^0(\omega, \mathbf{r}, \mathbf{r}'') \hat{V}(\omega, \mathbf{r}'') \hat{S}_F^0(\omega, \mathbf{r}'', \mathbf{r}') \quad (\text{B5})$$

where

$$\hat{S}_F^0(\omega, \mathbf{r}, \mathbf{r}') = \int \frac{d^2 k}{(2\pi)^2} \left(\frac{\gamma^0 \omega - \gamma^j k_j}{\omega^2 - k^2 + i\delta} \right) e^{-i\mathbf{k}(\mathbf{r}-\mathbf{r}')} \quad (\text{B6})$$

is the free fermion propagator. Writing the function Λ as

$$\Lambda(\mathbf{r}'') = \int \frac{d^2 p}{(2\pi)^2} e^{i\mathbf{p}\mathbf{r}''} \Lambda(\mathbf{p}),$$

we can use (B6) (B5) and integrate out the \mathbf{r}'' variable. We then take the limit $\mathbf{r}' \rightarrow \mathbf{r}$ and the trace of (B5) and get

$$\text{Tr} \hat{S}_F^1(\omega, \mathbf{r}, \mathbf{r}) = \frac{\mu}{2\pi^3 v_F^2} \int d^2 p e^{i\mathbf{p}\mathbf{r}} \Lambda(\mathbf{p}) \Gamma(\omega, \mathbf{p}), \quad (\text{B7})$$

with

$$\Gamma(\omega, \mathbf{p}) = \int d^2 q \frac{8\omega^3 - 2\omega q^2}{(\omega^2 - q^2 + i\delta)(\omega^2 - (q - p)^2 - i\delta)},$$

and

$$\Lambda(\mathbf{p}) = \sum_{i=1}^N \frac{e^{i\mathbf{p}\mathbf{x}_i}}{p^2}.$$

The correction to the local density of states comes from the imaginary part of equation (B7). This yields:

$$\delta N(\omega, \mathbf{r}) = \frac{\mu}{2\pi^3 v_F^2} 2\omega \Sigma_{i=1}^N \int dk \frac{J_0(\omega r_i)}{k^2} (4\omega^2 - k^2) F(\omega, k), \quad (\text{B8})$$

where the function $F(\omega, k)$ is

$$F(\omega, r) = \left\{ \begin{array}{ll} \frac{-\operatorname{atanh}(\frac{\sqrt{k^2 - 4\omega^2}}{k})}{\sqrt{k^2 - 4\omega^2}}, & 4\omega^2 < k^2 \\ \frac{\operatorname{atan}(\frac{k}{\sqrt{4\omega^2 - k^2}})}{\sqrt{4\omega^2 - k^2}}, & 4\omega^2 > k^2 \end{array} \right\}.$$

-
- [1] K. S. Novoselov, A. K. Geim, S. V. Morozov, D. Jiang, M. I. Katsnelson, I. V. Grigorieva, S. V. Dubonos, and A. A. Firsov, *Nature* **438**, 197 (2005).
 - [2] Y. Zhang, Y.-W. Tan, H. L. Stormer, and P. Kim, *Nature* **438**, 201 (2005).
 - [3] Y. Kopelevich, P. Esquinazi, J. H. S. Torres, R. R. da Silva, and H. Kempa, *Advances in Solid State Physics* **43**, 207 (2003).
 - [4] J. González, F. Guinea, and M. A. H. Vozmediano, *Phys. Rev. Lett.* **77**, 3589 (1996).
 - [5] G. V. Semenoff, *Phys. Rev. Lett.* **53**, 2449 (1984).
 - [6] F. D. M. Haldane, *Phys. Rev. Lett.* **61**, 2015 (1988).
 - [7] H. Kempa, P. Esquinazi, and Y. Kopelevich, *Solid State Communication* p. to appear (2006).
 - [8] P. Esquinazi, D. Spemann, R. Höhne, A. Setzer, K.-H. Han, and T. Butz, *Phys. Rev. Lett.* **91**, 227201 (2003).
 - [9] A. W. W. Ludwig, M. P. A. Fisher, R. Shankar, and G. Grinstein, *Phys. Rev. B* **50**, 7526 (1994).
 - [10] A. A. Nersesyan, A. M. Tsvelik, and F. Wenger, *Phys. Rev. Lett.* **72**, 2628 (1994).
 - [11] A. A. Nersesyan, A. M. Tsvelik, and F. Wenger, *Nucl. Phys. B* **438**, 561 (1995).
 - [12] T. Stauber, F. Guinea, and M. A. H. Vozmediano, *Phys. Rev. B* **71**, 041406(R) (2005).
 - [13] N. M. R. Peres, F. Guinea, and A. H. C. Neto, *Phys. Rev. B* (2006).
 - [14] N. Park, M. Yoon, S. Berber, J. Ihm, E. Osawa, and D. Tomanek, *Phys. Rev. Lett.* **91**, 237204 (2003).
 - [15] A. V. Rode, E. G. Gamaly, Christy, J. G. F. Gerald, S. T. Hyde, R. G. Elliman, B. Luther-Davies, A. I. Veinger, J. Androulakis, and J. Giapintzakis, *Phys. Rev. B* **70**, 054407 (2004).
 - [16] A. Hashimoto, K. Suenaga, A. Gloter, K. Urita, and S. Iijima, *Nature* **430**, 870 (2004).
 - [17] M. Ge and K. Sattler, *Chem. Phys. Lett.* **220**, 192 (1994).
 - [18] A. Krishnan, E. Dujardin, M. M. J. Treacy, J. Hugdahl, S. Lynam, and T. W. Ebbesen, *Nature* **388**, 451 (1997).
 - [19] H. Terrones, M. Terrones, and J. L. Morán-López, *Current Science* **81**, 1011 (2001).
 - [20] J. A. Jaszczaka, G. W. Robinson, S. Dimovskic, and Y. Gogotsic, *Carbon* (2003).
 - [21] B. An, S. Fukuyama, K. Yokogawaa, M. Yoshimura, M. Egashira, Y. Korai, and I. Mochida, *Applied Physics Letters* **78**, 3696 (2001).
 - [22] B. An, S. Fukuyama, K. Yokogawaa, M. Yoshimura, M. Egashira, Y. Korai, and I. Mochida, *Appl. Phys. Lett.* **23** (2001).
 - [23] Y. Lu, M. Munoz, C. S. Steplecaru, C. Hao, M. Bai, N. García, K. Schindler, and P. Esquinazi (2006), to appear in *Phys. Rev. Lett.*, cond-mat/0604280.
 - [24] P. R. Wallace, *Phys. Rev.* **71**, 622 (1947).
 - [25] J. C. Slonczewski and P. R. Weiss, *Phys. Rev.* **109**, 272 (1958).
 - [26] J. González, F. Guinea, and M. A. H. Vozmediano, *Phys. Rev. Lett.* **69**, 172 (1992).
 - [27] J. González, F. Guinea, and M. A. H. Vozmediano, *Nucl. Phys. B* **406** [FS], 771 (1993).
 - [28] J. González, F. Guinea, and M. A. H. Vozmediano, *Nucl. Phys. B* **424** [FS], 595 (1994).
 - [29] J. González, F. Guinea, and M. A. H. Vozmediano, *Phys. Rev. B* **63**, 134421 (2001).
 - [30] L. H. Ryder, *Quantum field theory* (Cambridge University Press, 1996).
 - [31] C. Furtado, F. Moraes, and A. M. de M. Carvalho (2006), cond-mat/0601391.
 - [32] P. E. Lammert and V. H. Crespi, *Phys. Rev. Lett.* **85**, 5190 (2000).
 - [33] V. A. Osipov and E. A. Kochetov, *Pisma v ZhETF* **73**, 631 (2001), english translation: *JETP Lett.* **73**, 562 (2001).
 - [34] R. Tamura and M. Tsukada, *Phys. Rev. B* **49**, 7697 (1994).
 - [35] J. C. Charlier and G. M. Rignanese, *Phys. Rev. Lett.* **86**, 5970 (2001).
 - [36] A. Vilenkin and E. P. S. Shellard, *Cosmic Strings and Other Topological Defects* (Cambridge University Press, 2000).
 - [37] A. N. Aliev, M. HÖrtacsu, and N. Ozdemir, *Class. Quantum. Grav.* **14** (1997).
 - [38] Birrell and Davis, *Quantum fields in curved space* (Cambridge University Press, 1982).

- [39] V. M. Pereira, F. Guinea, J. M. B. L. dos Santos, N. M. R. Peres, and A. H. C. Neto, Phys. Rev. Lett. **96**, 036801 (2006).
- [40] S. Azevedo, C. Furtado, and F. Moraes, Physica Status Solidi b **207** (1998).
- [41] A. J. Stone and D. J. Wales, Chem. Phys. Lett. **128** (1986).
- [42] P. M. Ajayan, V. Ravikumar, and J.-C. Charlier, Phys. Rev. Lett. **81** (1998).
- [43] L. Chico, L. X. Benedict, S. G. Louie, and M. L. Cohen, Phys. Rev. B **54** (1996).
- [44] M. Igami, K. Nakada, M. Fujita, and K. Kusakabe, Czech. J. Phys. **46** (1996).
- [45] E. J. Duplock, M. Scheffler, and P. J. D. Lindan, Phys. Rev. Lett. **92** (2004).